BAYESIAN TEXTURE BASED ANALYSIS OF HR SLC SAR IMAGES

Matteo Soccorsi[1] **and Mihai Datcu**[1,2]

[1]*DLR, German Aerospace Center, Oberpfaffenhofen, D-82234 Wessling, Germany*
[2]*ENST, École Nationale Supérieure des Tèlécommunications, 46 rue Barrault, 75634 Paris Cedex 13, France*

ABSTRACT

The Bayesian approach is a promising method for model-based signal analysis. It was previously used on detected radar images for model based despeckling and feature extraction. We propose an extension on Single Look Complex (SLC) High Resolution (HR) Synthetic Aperture Radar (SAR) images. The information contained in the phase is reflected in the second order statistics and it is important for texture characterization. The SLC data, generally modeled as circular complex Gaussian, is assumed to be modeled by a complex Gauss-Markov Random Fields (GMRF). An efficient parameter extraction for texture characterization is important in order to create an alphabet of plausible primitive feature for image labeling. The affectation of the phase correlation on parameter estimation is explored. The results are demonstrated on E-SAR SLC HR images.

Key words: Synthetic Aperture Radar (SAR); Gauss-Markov Random Field (GMRF); primitive feature extraction; texture.

1. INTRODUCTION

Texture is an important feature for image analysis. Although it is easy to recognize it has many different definitions spanning visual up to statistical properties description. In computer vision the texture is a 2D quasi repetitive structure looking like a material, some examples can be brick wall, skin, stone, metal or wood surfaces. In computer graphic the texture is the property (in terms of light and shade) of a surface or an object to look like made by a certain material. There are many examples in 3D game design. In Earth Observation (EO) optical images texture definition comes directly from the previous ones. Forests, meadows, land, water, cities are examples of textures at low resolution acquisition.
In the HR SAR images texture must be redefined because it is not anymore characterizing the optical features but the electromagnetic property of the illuminated targets. It basically distinguishes the optical from the SAR images and makes the interpretation of the latter a difficult task, because what we see is not what the human eye expects to see.
The content of the SAR image is characterize from a its own geometry which differs from the real geometry of the illuminated scene and it is dominated from strong scatterers. Nevertheless we are going to accept the classical texture definition in homogeneous areas, but we are going to extend it for a characterization of isolated and structured objects, too.
The task in SAR is to detect and recognize objects and structures thus we redefined the texture as a local descriptor of the scatterers and structured scatterers: the contextual information as spatial descriptor in small window surrounding the pixels. Since texture information is a descriptor of the scene structures and objects, texture parameters are important for the recognition of HR SAR images: for classification as separation of different textures and for object recognition as fingerprint and local diversity characterization.
Following [Chelappa85] and [Sekita92] we propose a new complex GMRF for direct model SLC data. The information delivered from the phase is described in the second order statistics and it is important for texture characterization. Thus, the circular complex Gaussian model of the data is extended to be modeled by GMRF. An efficient parameter extraction for texture characterization is important in order to create an alphabet of plausible primitive feature for image labeling. A Bayesian parameters estimation and model selection is implemented and compared with Evidence Maximization information extraction [Walessa00].
The paper is structured as follows: Section II introduces an overview of SAR principles and imaging features; Section III gives an overview of Bayesian inference and parameter estimation; in Section IV the observed model and the image model are defined; Section V reports the implementation aspects; Section VI presents experimental results and Section VI ends the paper with some conclusion.

2. SAR OVERVIEW

A simplified end-to-end SAR system is shown in Fig. 2. The complex reflectivity function $x(r,t)$ is convoluted with the end-to-end SAR system impulse response $s(r,t)$ for giving the complex scene $y(r,t)$ and then the detected

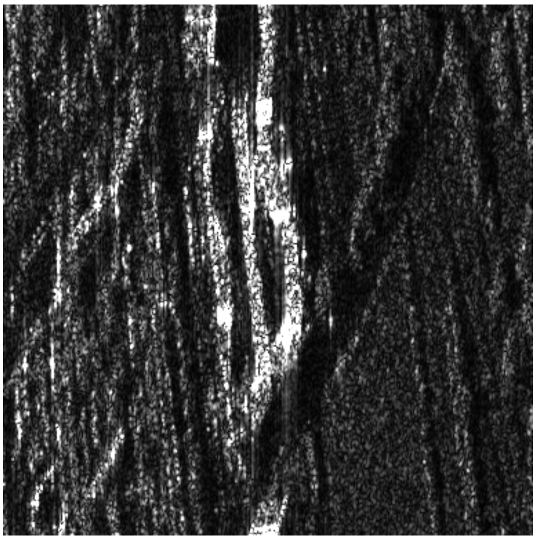

Figure 1. SLC amplitude image.

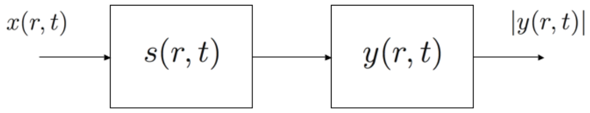

Figure 2. End-to-end SAR system.

real image $|y(r,t)|$. The variable r defines the position in range and the variable t (time) is the position in azimuth [Schreier93]. The end-to-end SAR imaging system model is essentially a linear range-invariant filter:

$$y(r,t) = x(r,t) * s(r,t) \tag{1}$$

where the symbol $*$ denotes the convolution. In Figs. 1 and 3 are shown example of SLC amplitude and phase image. Because of the property of the phase which is uniform distributed, up to now it was neglected and the efforts were concentrated on the quantity $|y(r,t)|$ [Lopés90] and [Datcu98]. The detected image is affected by the so-called speckle noise, which is a deterministic effect due to coherent nature of SAR imaging: when the number of scatterers within a surface resolution cell is very large and their distribution in height occurs on a scale of wavelength or grater, the speckle is referred to as fully developed [Dainty75].

With the advent of HR SAR sensor the condition for fully developed speckle is not anymore respected and the phase shows correlation patterns (see Fig. 3) which brings information on the scene. Thus the necessity of moving from the detected to the SLC image for a complete image characterization.

The complex valued data $y = y_{re} + j \cdot y_{im}$ are modeled by GMRF. It brings to an easier modeling and a linear parameter estimation ensuring a less complexity and faster algorithm. We compared the results with the Evidence Maximization algorithm with our algorithm.

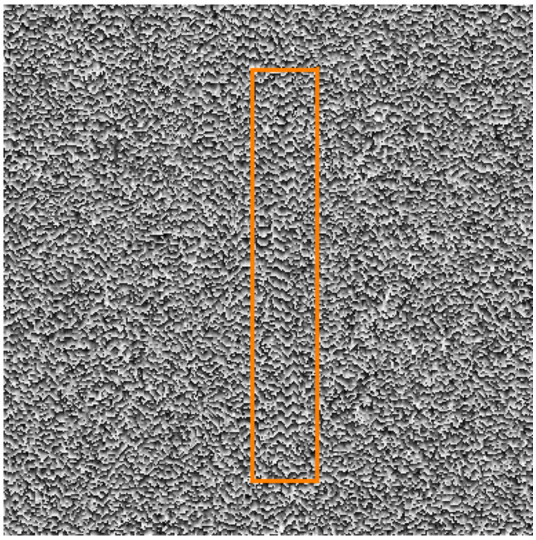

Figure 3. SLC phase image.

3. BAYESIAN INFERENCE

In Bayesian probability theory, logical link is expressed by conditional probability distribution $p(\boldsymbol{x}|\boldsymbol{y}) = p(\boldsymbol{x},\boldsymbol{y})/p(\boldsymbol{y})$. It expresses the degree of belief that the event $\boldsymbol{x}$ takes place given the occurrence of the event $\boldsymbol{y}$. Where $\boldsymbol{y}$ is the image observed values corrupted by the noise $\boldsymbol{n}$ and $\boldsymbol{x}$ are the parameters we want to estimate. An immediate consequence of the definition of conditional probability is the Bayes' law:

$$p(\boldsymbol{x}|\boldsymbol{y}) = \frac{p(\boldsymbol{y}|\boldsymbol{x})p(\boldsymbol{x})}{p(\boldsymbol{y})}, \tag{2}$$

which enables the reversal of probabilistic link and therefore it allows a direct model based inference. The law can be seen as a rule for updating an existing description, the prior $p(\boldsymbol{x})$, of a phenomenon $\boldsymbol{x}$, based on new information-new data or new description of the phenomenon $\boldsymbol{y}$. The direct link from old to new description is modeled by the likelihood $p(\boldsymbol{y}|\boldsymbol{x})$. Furthermore, the evidence normalization term, $p(\boldsymbol{y})$, describes the distribution of the data given the model and it can be computed by marginalization:

$$p(\boldsymbol{y}) = \int p(\boldsymbol{y}|\boldsymbol{x})p(\boldsymbol{x})d\boldsymbol{x}. \tag{3}$$

where the integral is over all the parameter space. The evidence has a main role in model selection.

3.1. Overview on Parameter Estimation

The importance of the estimation error in a certain application, is measured using a *cost function*. It can assume different forms:

$$c_q = (\boldsymbol{x} - \hat{\boldsymbol{x}})^2 \tag{4}$$

$$c_u = \begin{cases} 0 & \text{for} \quad |\boldsymbol{x} - \hat{\boldsymbol{x}}| \leq \tau/2 \\ 1 & \text{for} \quad |\boldsymbol{x} - \hat{\boldsymbol{x}}| > \tau/2 \end{cases} \tag{5}$$

where c_q is the quadratic cost function and c_u is the uniform one with τ a fixed threshold. The expectation of the cost relative to the joint probability density function (p.d.f.) $p(\boldsymbol{x}, \boldsymbol{y})$ is called *Bayes risk*:

$$R = \mathrm{E}\Big[c(\boldsymbol{x} - \hat{\boldsymbol{x}})\Big] = \iint c(\boldsymbol{x} - \hat{\boldsymbol{x}}) p(\boldsymbol{x}, \boldsymbol{y}) d\boldsymbol{x} d\boldsymbol{y} \tag{6}$$

where the notation E[.] expresses the expectation operation.
The quadratic cost function (4) leads to the Minimum Mean Squared Error (MMSE) estimator:

$$\hat{\boldsymbol{x}}_{\mathrm{MMSE}} = \int \boldsymbol{x} p(\boldsymbol{x}|\boldsymbol{y}) d\boldsymbol{x}. \tag{7}$$

The MMSE estimator is the conditional mean and it is a function of the observation $\hat{\boldsymbol{x}}_{\mathrm{MMSE}}(\boldsymbol{y})$.
The choice of the uniform cost function (5) brings to the Maximum *A Posteriori* (MAP) estimator:

$$\hat{\boldsymbol{x}}_{\mathrm{MAP}} = \arg\max_{\boldsymbol{x}} p(\boldsymbol{x}|\boldsymbol{y}) \tag{8}$$

where the posterior can be evaluated using the Bayes formula (2). We observe that even if both the estimators use the posterior p.d.f. $p(\boldsymbol{x}|\boldsymbol{y})$, however the estimators extract different information and do not result in the same solution. The MMSE is the center of mass, while the MAP is the mode of the p.d.f.
When the parameter to be estimated is unknown but deterministic the prior p.d.f. is a delta function $p(\boldsymbol{x}) = \delta(\boldsymbol{x} - \boldsymbol{x}_0)$. It makes the definition of the risk inconsistent, then we introduce the likelihood function $L(\boldsymbol{x})$ defined as follows:

$$L(\boldsymbol{x}) = p(\boldsymbol{y}|\boldsymbol{x}) \tag{9}$$

It reaches its maximum when the noise is zero with high probability. This leads to the Maximum Likelihood (ML) estimator:

$$\boldsymbol{x}_{ML} = \arg\max_{\boldsymbol{x}} p(\boldsymbol{y}|\boldsymbol{x}). \tag{10}$$

Some observations must be done on the above estimators:

- if the posterior $p(\boldsymbol{x}|\boldsymbol{y})$ is symmetric then $\boldsymbol{x}_{MAP} = \boldsymbol{x}_{MMSE}$, and
- if the prior $p(\boldsymbol{x})$ is uniform then $\boldsymbol{x}_{MAP} = \boldsymbol{x}_{ML}$

We can conclude that MAP estimate is a complete frame for model-based approaches in information extraction. It is equivalent to Minimum Description Length (MDL) [Rissanen85] which states that the best model of a phenomenon is the one producing the most compact encoding of it. Similarly to MDL, the Akaike Information Criterion (AIC) [Akaike74] considers two terms: a data one, requiring likelihood maximization, and a penalty one, weighting the complexity of the model.

	x_{44}	x_{32}	x'_{41}	
x_{43}	x_{22}	x_{12}	x'_{21}	x'_{42}
x_{31}	x_{11}	x_s	x'_{11}	x'_{31}
x_{42}	x_{21}	x'_{12}	x'_{22}	x'_{43}
	x_{41}	x'_{32}	x'_{44}	

Figure 4. Example of neighborhood $\mathcal{N}$.

NEIGHBORHOOD	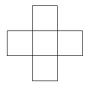 $\mathcal{N}'$		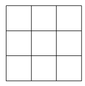 $\mathcal{N}''$			
CLIQUES	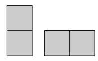		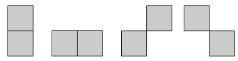			
PARAMETERS	θ_1	θ_2	θ_1	θ_2	θ_3	θ_4

Table 1. First and second model order with the clique system and the correspondent parameters.

4. MODELING SLC SAR DATA

The observation model comes from the SAR imaging system. Let

$$\boldsymbol{y} = \{y_i \in \mathbb{C} \mid i = 1, \ \ldots \ M \times N\} \tag{11}$$

be the $M \times N$ observed image with $y_i = y_i^{re} + j \cdot y_i^{im}$ row by row lexicographic indexed pixels. Thus the observation model is given by:

$$\boldsymbol{y} = f(\boldsymbol{x}) + \boldsymbol{n} \tag{12}$$

with $\boldsymbol{n}$ additive Gaussian white noise. From (12) we can obtain the following conditional density distribution of the observation y_i respect to the occurrence of x_i:

$$p(y_i|x_i) = \frac{1}{2\pi\sigma_i^2} \exp\left\{-\frac{(y_i^{re} - x_i^{re})^2 (y_i^{im} - x_i^{im})^2}{2\sigma_i^2}\right\} \tag{13}$$

which is representative of a circular complex Gaussian distributed phenomenon with space variant variance noise σ_i.

4.1. Image Model

We model the image as GMRF, defined as follows [Chelappa93]:

$$p(\boldsymbol{x}) = \frac{1}{(2\pi)^{MN} \det(\boldsymbol{\Sigma})} \exp\{-\frac{1}{2}\boldsymbol{x}^T [\boldsymbol{\Sigma}]^{-1} \boldsymbol{x}\} \tag{14}$$

where:

$$\boldsymbol{x} = \{x_i \in \mathbb{C} \mid i = 1, \ \ldots \ M \times N\} \tag{15}$$

is the lexicographic ordered array of the real complex reflectivity function and $\mathbf{\Sigma}$ is the covariance matrix of the data. Equation (14) is the quadratic form for a multivariate complex Gaussian distribution, which can be also written as the following conditional distribution [Chelappa93]:

$$p(x_s|\mathcal{N}, \boldsymbol{\theta}) = \frac{1}{2\pi\sigma^2}\exp\{-\frac{1}{2\sigma^2}[x_s - \eta]^2\} \quad (16)$$

$$\eta = \sum_{i,j\in\mathcal{N}} \theta_{ij}(x_{ij} + x'_{ij}) \quad (17)$$

where the subindex s and the indexing ij refer to Fig. 4 where is shown an example of neighborhood $\mathcal{N}$ and σ^2 is the variance of the noise. $\boldsymbol{x}_s \subset \boldsymbol{x}$ is the subset of central pixels for complete neighborhoods:

$$\boldsymbol{x}_s = \{x_i \in \mathbb{C} \mid x_i \in \mathcal{N}\}. \quad (18)$$

Equation (16) comes from the conjoint Gaussian distribution of independent random variables and from the Hammersley-Clifford theorem which proofs the dependency of each central pixel value to the values of a limited number of surrounding pixels (neighborhood concept). Then writing the model as a conditional distribution function is possible, where the conditioning is on the neighborhood and on the clique system which together define the model order (see Table 1).

5. IMPLEMENTATION ASPECTS

5.1. GMRF as Linear Predictor

The GMRF model can be written in the form:

$$x_s = \sum_{i,j\in\mathcal{N}} \theta_{ij}(x_{ij} + x'_{ij}) + n \quad (19)$$

where the same notation of eqs. (16) and (17) and referred to Fig.: 4 was used, with x_s the center of the neighborhood and n zero-mean white Gaussian noise. By considering eq. (12) we can rewrite (19) in matrix form:

$$\boldsymbol{x}_s = \mathbf{G}\boldsymbol{\theta} + \boldsymbol{n} \quad (20)$$

where $\mathbf{G}$ is the matrix of the cliques, $\boldsymbol{\theta}$ is the parameter vector and $\boldsymbol{x}_s$ is the noisy image. The number of lines of the matrix $\mathbf{G}$ is equal to the number of elements P of the set $\boldsymbol{x}_s$ and the number of columns, depending on the model order, is equal to the dimension of the parameter vector. An example of construction of $\mathbf{G}$ matrix for Gauss-Markov model of 2nd order is given in Fig. 5 [Datcu04].

5.2. Least Squares Estimator (LSE)

We are interested in the estimation of the parameter vector $\boldsymbol{\theta}$. Since we consider a linear Gaussian model,

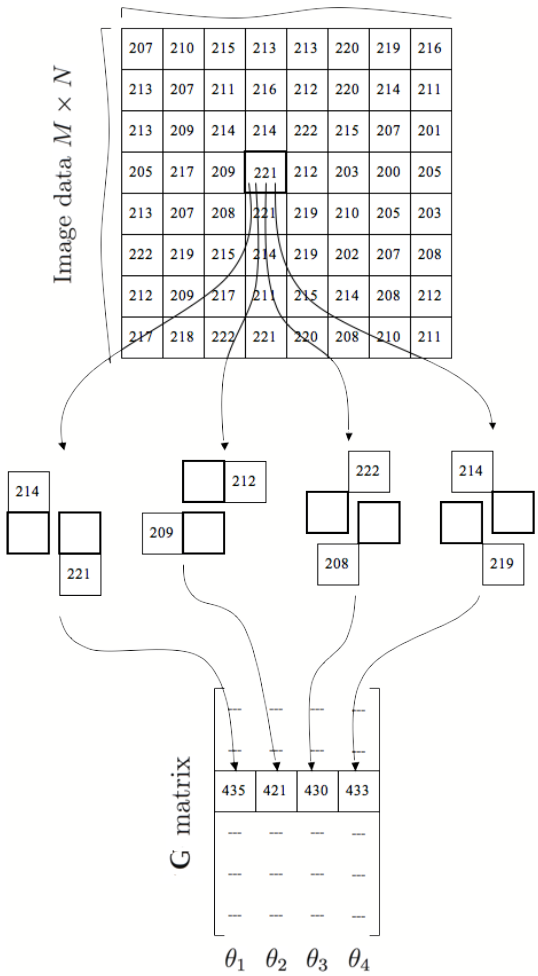

Figure 5. Example of $\mathbf{G}$ *matrix for Gauss-Markov model of 2nd order.*

due to the symmetry of the Gaussian p.d.f. we have $\boldsymbol{\theta}_{MAP} = \boldsymbol{\theta}_{MMSE}$. Moreover we consider as prior for the parameter vector $\boldsymbol{\theta}$ a uniform p.d.f. ($\boldsymbol{x}_{MAP} = \boldsymbol{x}_{ML}$) and uncorrelated Gaussian noise, because no prior knowledge is available and then the simplest assumption is done. Thus, this results in the LSE, which takes the form [Ruanaidh96]:

$$\hat{\boldsymbol{\theta}} = \left(\mathbf{G}^T\mathbf{G}\right)^{-1}\mathbf{G}^T\boldsymbol{x}_s \quad (21)$$

where $\hat{\boldsymbol{\theta}}$ is the estimated parameter vector and the notation is coherent with eq. 20.

5.3. Variance of the model

We also computed the variance of the model as follows:

$$\sigma^2 = \frac{1}{P}\sum_{s=1}^{P}(\boldsymbol{x}_s - \boldsymbol{\epsilon})^2 \quad (22)$$

$$\boldsymbol{\epsilon} = \mathbf{G}\hat{\boldsymbol{\theta}} \quad (23)$$

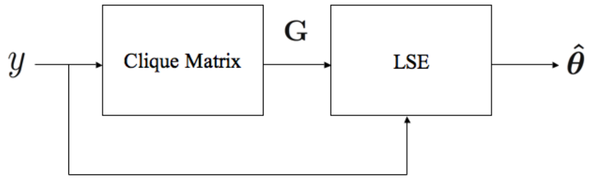

Figure 6. Algorithm block diagram.

where P is the number of elements of the subset $\boldsymbol{x}_s$ and ϵ is the best fit of the data.

5.4. Evidence of the model

In case of GMRF the evidence of the model takes the following form [Ruanaidh96]:

$$p(y_i|H) = \tag{24}$$

$$\frac{\pi^{-N/2}\Gamma\left(\frac{Q}{2}\right)\Gamma\left(\frac{P-Q}{2}\right)\det\left([\boldsymbol{G}]^T[\boldsymbol{G}]\right)^{-1/2}}{4\kappa\left(\hat{\boldsymbol{\theta}}^T\hat{\boldsymbol{\theta}}\right)^{Q/2}\left(\boldsymbol{x}^T\boldsymbol{x}-\boldsymbol{\epsilon}^T\boldsymbol{\epsilon}\right)^{(P-Q)/2}} \tag{25}$$

where $\Gamma(\cdot)$ is the Gamma function, Q is the dimension of the parameter vector $\boldsymbol{\theta}$, κ is a normalization constant and $\boldsymbol{\epsilon}$ is defined in eq. (23).

6. APPLICATION

We applied the method on an E-SAR scene of Dresden city, Germany. Six parameters, corresponding to a model of third order, were estimated and then the variance and the evidence were calculated as described in section V. One exemplified image is shown in Fig. 1. As remarked the phase presents correlation patterns as highlighted in the phase image in Fig. 3. The extracted texture parameters are shown in Fig. 7 and the evidence and the variance of the model are presented in Fig. 8. Both of them show the building and the strong scatterers. The goodness of the results was qualitatively evaluated by classification.
The classification on the feature space was performed with the unsupervised K-Means. The result of the classification is shown in Fig. 9 for five classes. In order to investigate the sensitivity of the model to phase correlation, we applied the method on unitary constant amplitude data. The evidence of the model is able to capture the phase correlation as shown in Fig. 10. We observed that some parameters show phase structures which are not visible in the wrapped phase of Fig. 3. The two relevant unitary constant amplitude parameters are shown in Fig. 11: the white part reveals a correlation in the phase. We have to investigate if the model is able to capture not evident phase pattern or they are artifact.

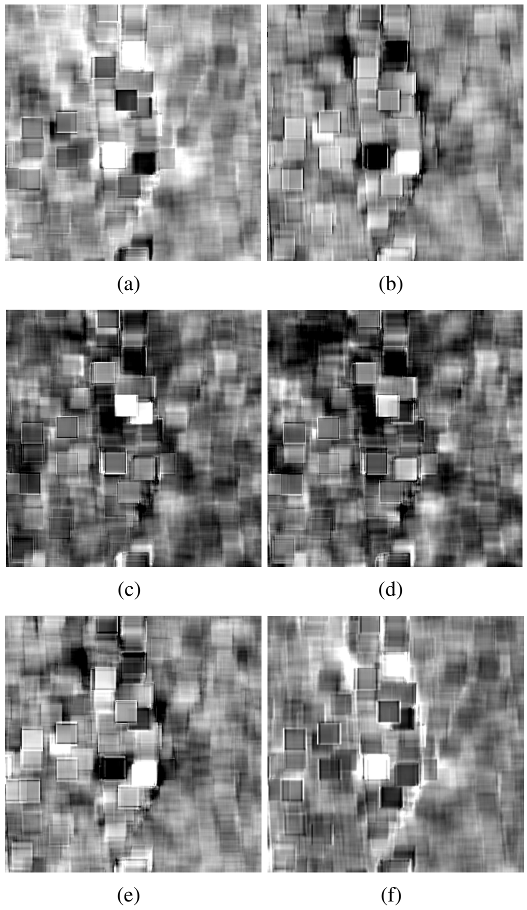

Figure 7. Parameter vector. Clique: (a) vertical, (b) horizontal, (c) $+45^o$ diagonal, (d) -45^o diagonal, (e) vertical and (f) horizontal with a jump of one pixel.

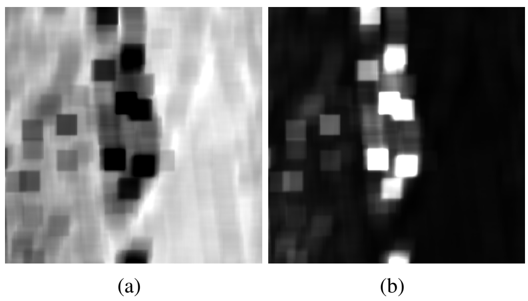

Figure 8. (a) evidence and (b) variance of the model.

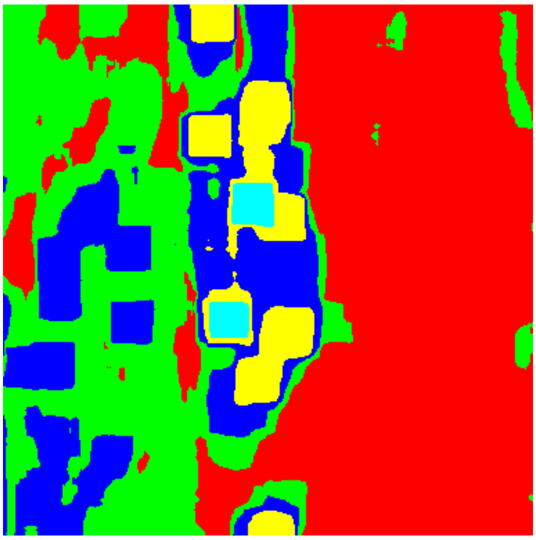

Figure 9. Classification map. Meadows and asphalt (red), small structures and vegetation (green), buildings (blue), big buildings (yellow), very strong scatterers (light blue).

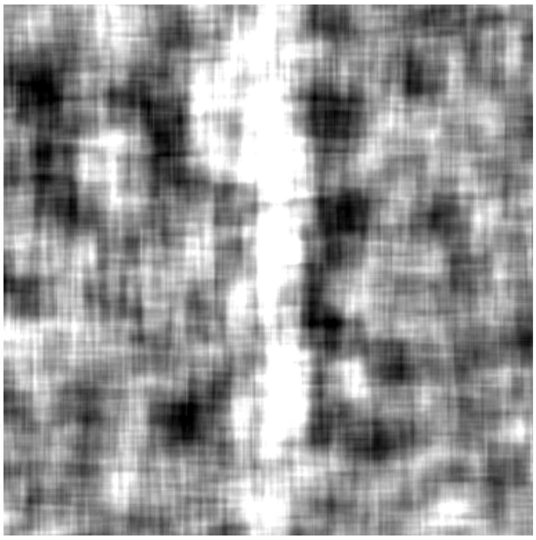

Figure 10. Evidence for unitary constant amplitude shows the correlation pattern in phase.

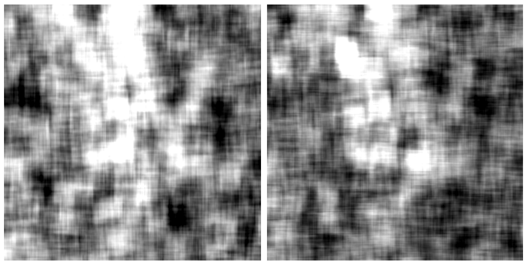

(a) (b)

Figure 11. Parameters for constant unitary amplitude. Clique: (a) vertical and (b) horizontal with jump of one pixel.

6.1. Evidence Maximization Comparison

The comparison with the Evidence Maximization algorithm [Walessa00] shows that we obtained best results with the complex GMRF. This is due to the different resolution since the image must be under-sampled to decorrelated the speckle noise and to the phase information which is neglected by Evidence Maximization but is taking into account from our algorithm. Moreover because of the linearity, the complexity of the algorithm is lower and it results in a reduction of the computation time of one order of magnitude.

7. CONCLUSION

For SLC images the circular complex Gaussian model is easier to treat then the Gamma model for detected images and this results in a faster algorithm, it brings to a linear model selection and parameter estimation. Moreover it permits to exploit the information contained in the phase which is not anymore neglectable in HR images because it delivers information on the scene phase second order statistics. In the article it is demonstrated that GMRF is able to capture and model the amplitude behavior together with the phase correlation.

ACKNOWLEDGMENT

This work was carried out in the frame of the *CNES/DLR/ENST Center of Competence on information extraction and image understanding for Earth Observation*. The authors would like to thank Gottfried Schwarz for the worthwhile contribution.

REFERENCES

[Akaike74] H. Akaike, *A New Look at the Statistical Model Identification*, IEEE Transactions on Autom. Control, vol. 19, pp. 716-723, June 1974.

[Chelappa85] R. Chelappa, S. Chatterjee and R. Bagdazian *Texture Synthesis and Compression Using Gaussian-Markov Random Field Models* IEEE Trans. Syst., Man, Cybern., vol. SMC-15, no. 2, pp. 298-303, March/April 1985.

[Chelappa93] R. Chelappa and A. Jain, *Markov Random Fields: Theory and Application*, Academic Press, pp. 131-157, San Diego, CA, 1993.

[Dainty75] J. C. Dainty, *Laser Speckle and Related Phenomena*, Springer-Verlag Berlin Heidelberg New York, pp. 9-76, 1975

[Datcu98] M. Datcu, K. Seidel and M. Walessa, *Spatial Information Retrieval From Remote Sensing Im-*

ages: Part A. Information Theoretical Perspective, IEEE Trans. Geosci. Remote Sens., vol. 36, pp. 1431-1445, Dec. 1998.

[Datcu04] M. Datcu, D. A. Stoichescu, K. Seidel, C. Iorga, *Model Fitting and Model Evidence for Multiscale Image Texture Analysis*, Proc. International Workshop on Bayesian Inference and Maximum Entropy Methods in Science and Engineering MaxEnt, pp. 35-42, Garching, Germany, 2004.

[Lopés90] A. Lopés, R. Touzi and E. Nezry, *Adaptive Speckle Filters and Scene Heterogeneity*, IEEE Trans. Geosci. Remote Sens., vol. 28, pp. 992-1000, Nov. 1990.

[Rissanen85] J. Rissanen, *Minimum Description Length Principle*, Encyclopedia of Statistical Sciences, vol. 5, pp. 523-527, Wiley, New York, 1985.

[Ruanaidh96] J. Ruanaidh, W. Fitzgerald, *Numerical Bayesian Methods Applied to Signal Processing*, Springer-Verlag, New York, 1996.

[Schreier93] G. Schreier, *SAR Geocoding: Data and Systems*, Herbert Wichmann Verlag GmbH, pp. 53-102, Karlsruhe, 1993.

[Sekita92] I. Sekita, T. Kurita, N. Otsu, *Complex Autoregressive Model for Shape Recognition*, IEEE Trans. Pattern Anal. Mach. Intell., vol. 14, pp. 489-496, Apr. 1992.

[Walessa00] M. Walessa, M. Datcu, *Model-Based Despeckling and Information Extraction from SAR Images*, IEEE Trans. Geosci. Remote Sens., vol. 38, pp. 2258-2269, Sept. 2000.